JOURNAL OF COMPUTATIONAL PHYSICS 28, 1–13 (1978)

Comparative Numerical Studies of Ideal Magnetohydrodynamic Instabilities

M. S. CHANCE, J. M. GREENE, R. C. GRIMM,
J. L. JOHNSON,* AND J. MANICKAM

Princeton University Plasma Physics Laboratory, Princeton, New Jersey 08540

W. KERNER

Max-Planck-Institut für Plasmaphysik, Garching, Germany

AND

D. BERGER, L. C. BERNARD, R. GRUBER, AND F. TROYON

École Polytechnique Fédérale de Lausanne, Lausanne, Switzerland

Received May 31, 1977; revised August 17, 1977

Stability properties associated with a specific analytic equilibrium have been calculated to compare the accuracy of three large computational programs that have been developed at Garching, Princeton, and Lausanne. All three use a Galerkin formulation of the variational principle for determining spectra. Good agreement is found, verifying the efficacy of all three codes.

1. INTRODUCTION

The investigation of the ideal magnetohydrodynamic stability properties of tokamak devices is an essential part of current thermonuclear research. We discuss and compare three independent programs that have been developed to investigate the eigenspectrum for such devices in an ideal model: (1) the Garching–Princeton code (KERNER) [1]; (2) the Princeton Equilibrium, Stability, and Transport code (PEST) [2]; and the Lausanne code (ERATO) [3]. This provides a series of cross checks that is essential for validating such large, complex programs. All three use a Lagrangian formalism for linearized perturbations to obtain a matrix eigenvalue problem. This is solved to obtain any desired portion of the spectrum and its associated set of normal modes. To make the comparison, we adopt a specific analytic equilibrium.

* On loan from Westinghouse Research and Development Center.

0021-9991/78/0281–0001$02.00/0

In Section 2 we give Solov'ev's equilibrium model [4] and describe some of its properties. This rather simple analytic model contains the essential features of a real plasma and provides a great deal of numerical and physical insight into what should be expected with a more realistic numerically determined equilibrium. We describe in Section 3 the similarities and differences with the three normal-mode programs. Some specific numerical comparisons are given in Section 4 and a discussion of the results in Section 5.

2. Equilibrium

When the pressure is contained solely by the toroidal current, the MHD equilibrium equation for the poloidal flux Ψ,

$$X \frac{\partial}{\partial X} \frac{1}{X} \frac{\partial \Psi}{\partial X} + \frac{\partial^2 \Psi}{\partial Z^2} = 2\pi X J_\phi = -4\pi^2 X^2 \frac{dp}{d\Psi} \tag{1}$$

with

$$\mathbf{B} = \frac{1}{2\pi} \nabla\phi \times \nabla\Psi + RB_0 \nabla\phi, \tag{2}$$

has the solution

$$\Psi = \frac{\pi B_0}{ER^2 q(0)} \left[X^2 Z^2 + \frac{E^2}{4} (X^2 - R^2)^2 \right] \tag{3}$$

if

$$p(\Psi) = \frac{(1 + E^2) B_0}{2\pi E R^2 q(0)} (\Psi_B - \Psi) \tag{4}$$

(see Fig. 1). Here (X, ϕ, Z) is a cylindrical coordinate system, B_0 is the toroidal field at the magnetic axis $X = R$, $p(\Psi)$ is the material pressure, and

$$q(\Psi) = RB_0 \oint [dl/X \mid \nabla\Psi \mid] \tag{5}$$

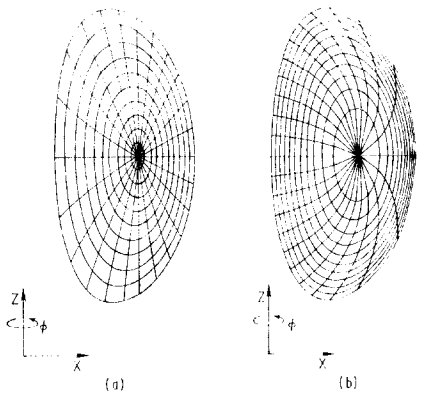

Fig. 1. Magnetic surfaces for a family of equilibria with $\epsilon = \frac{1}{3}$, $E = 2$, showing lines of constant ψ and θ for the coordinate systems used in the KERNER (a) and PEST (b) codes. The ERATO code uses ψ_k and θ_p as coordinates.

is the safety factor. The contour of integration is along a line of constant Ψ and ϕ. We characterize the system by the parameters E, $\epsilon \equiv [\Psi_B q(0)/\pi E R^2 B_0]^{1/2}$, and $q(0)$; E determines the ellipticity at the magnetic axis, ϵ fixes the aspect ratio, and $q(0)$ can be associated with the magnitude of the toroidal current.

3. Formulations

There has been considerable interaction between the groups that developed these three codes [1–3] for determining the spectrum and investigating instabilities of tokamak configurations. Thus there are similarities among them. Nevertheless, they have significant differences [5]. Since each has been carefully described, we merely comment on these similarities and differences.

A. *Equlibrium*

The KERNER code [1] utilizes the analytic properties of the equilibrium of Eq. (3) and is thus restricted in its application. Both the PEST code [2] and the ERATO code [3] can accept any equilibrium configuration for which $\Psi(X, Z)$ is specified on a rectangular mesh. An equilibrium routine [6] is an integral part of the PEST package. The ERATO code is interfaced to the Oak Ridge equilibrium solver [7].

B. *Coordinates*

All three codes use a nonorthogonal (ψ, θ, ϕ) flux coordinate system for the stability analysis. In the KERNER program $\psi_k \propto \Psi^{1/2}$ and $\theta_k \equiv \tan^{-1}[2XZ/E(X^2 - R^2)]$ such that the transformations to the new coordinates can be performed analytically. In the PEST code $\psi_p \propto \int d\tau/X^2$ and θ_p is chosen to make $\mathscr{J} \equiv (\nabla\psi_p \times \nabla\theta_p \cdot \nabla\phi)^{-1} \propto X^2$ so that the magnetic field lines appear to be straight. The ERATO code uses the KERNER flux label Ψ_k and the PEST angle θ_p. Both of these codes utilize a mapping routine [2] to determine $X(\psi, \theta)$ and $Z(\psi, \theta)$, given $\Psi(X, Z)$.

C. *Variational Approach*

The normal modes associated with linearized perturbations around the equilibrium are determined by making the Lagrangian

$$\mathscr{L} = \omega^2 K(\xi^*, \xi) - \delta W(\xi^*, \xi) \tag{6}$$

stationary with respect to the displacement vector ξ, with K and δW the kinetic and potential energy functionals [8]. A Galerkin method in which ξ is approximated by a superposition of J linearly independent expansion functions,

$$\xi^{(J)} = \sum_{j=1}^{J} a_j \Phi_j , \tag{7}$$

leads to the matrix eigenvalue problem

$$\sum_{j=1}^{J} (\omega^2 \langle \Phi_{j'}^* \mid K \mid \Phi_j \rangle - \langle \Phi_{j'}^* \mid \delta W \mid \Phi_j \rangle) a_j = 0. \tag{8}$$

D. *Decomposition of Eigenvectors and Expansion Functions*

Special care must be taken to provide an adequate description of the different branches of the spectrum when computing the normal modes. Thus, in each of the approaches a specific decomposition of the eigenfunctions and a special choice for the expansion functions has been developed. In each case, Fourier decomposition in ϕ; i.e., $\xi(\psi, \theta, \phi) = \sum_n \xi_n(\psi, \theta) \exp in\phi$, has been used since the symmetry of the equilibrium decouples modes with different n's.

The KERNER code uses modified eigenfunctions of the corresponding straight configuration [9] as expansion functions. Thus ξ is expanded in terms of three orthogonal vectors, corresponding to the fast magnetosonic, shear Alfvén, and slow sound branches;

$$\xi(\psi, \theta) = \sum_{l,\nu} (C_{l,\nu}^F \xi_{l,\nu}^F + C_{l,\nu}^A \xi_{l,\nu}^A + C_{l,\nu}^S \xi_{l,\nu}^S) \exp il\theta, \tag{9}$$

where the $\xi_{l,\nu}^I$'s are Bessel functions of ψ with ν nodes. Since these global functions reduce to the exact eigenfunctions in the large aspect ratio limit for a circular cross-section device, this provides sufficient separation of the branches. The expansion functions associated with the Alfvén branch $\xi_{l,\nu}^A$ satisfy $\nabla \cdot \xi / X^2 = 0$ exactly to guarantee good separation from the fast magnetosonic modes.

In the PEST code the decoupling of the different branches is accomplished by setting

$$\xi = \frac{\mathscr{J} \xi_\psi}{R^2 B_0} \nabla\theta \times \mathbf{B} + i \frac{\mathscr{J} \xi_s}{R^2 B_0} \mathbf{B} \times \nabla\psi + i \frac{\xi_b}{B_0} \mathbf{B} \tag{10}$$

with

$$\xi_\psi = \delta - 2\pi i \partial\zeta/\partial\theta, \qquad \xi_s = 2\pi \partial\zeta/\partial\psi, \tag{11}$$

and using ζ, δ, and ξ_b as independent variables. Then, the slow branch is associated primarily with parallel flow ξ_b, and the shear Alfvén branch with the stream function ζ for incompressible perpendicular flow. Using Fourier components in θ enables one to evaluate $\mathbf{B} \cdot \nabla\xi$ accurately on surfaces near where $l - nq(\psi) = 0$. Linear finite elements are used for the ψ-dependence of ζ and δ and piecewise constant functions for ξ_b. Then the errors in evaluating $\nabla \cdot \xi_\perp / X^2$ and $\nabla \cdot \xi$ are small.

Mercier's formulation of δW [10] is used in the ERATO code with the decomposition

$$\xi = X^2 \xi_\psi \nabla\phi \times \nabla\theta + \frac{X^2}{\psi} \xi_s \nabla\psi \times \nabla\phi + \frac{X^2}{\psi} \xi_b \mathbf{B}. \tag{12}$$

Finite elements are chosen as expansion functions in both ψ and θ. These coefficients are complex but because of mirror symmetry about the $Z = 0$ plane only those for

$\theta \leqslant \pi$ need be included. The potential energy δW is put in a form with four positive terms and one that can become negative. The expansion functions are chosen so that each term can vanish separately. These conditions cannot be satisfied everywhere with the usual finite elements. Therefore, the Lagrangian is written formally as depending on seven variables, ξ_ψ, $\partial\xi_\psi/\partial\psi$, $\partial\xi_\psi/\partial\theta$, ξ_s, $\partial\xi_s/\partial\theta$, ξ_b, and $\partial\xi_b/\partial\theta$, with the constraints that the derivatives be correctly approximated at the mesh points. The error introduced by this technique decreases with a finer resolution in the grid. The smallest eigenvalue converges from below to the exact value and the effective value of q is shifted by a quantity that vanishes with the mesh size. In the usual Lagrangian formalism, e.g., the KERNER and PEST codes, the convergence is from above.

E. *Vacuum Region*

In the KERNER code the perturbed magnetic field in the vacuum region is expressed in terms of a vector potential **A**. This is expanded in a set which consists of the solutions for the analogous straight system. The volume calculation is performed using the same coordinate system as in the plasma region. Thus, the vacuum boundary must be a perfectly conducting surface obtained by setting Ψ equal to a constant in Eq. (3). This surface has an aspect ratio ϵ_W defined in the same way as for the plasma boundary. It is parameterized by $\Lambda \equiv \epsilon_W/\epsilon_B = (\Psi_W/\Psi_B)^{1/2}$. Since this is not a flux surface in the vacuum, the equilibrium field must penetrate this wall. The vector potential is evaluated with a Galerkin procedure, taking into account the boundary conditions, and thus requiring a matrix inversion.

Both the PEST and ERATO codes express the perturbed field in the vacuum region in terms of a scalar potential and use Green's functions to determine the contribution to δW in terms of the normal component of ξ at the plasma–vacuum interface. Special care [2, 11] is taken to ensure that the flux constraints are satisfied.

In all three codes the normal component of the displacement vector can be made to vanish at the plasma surface, corresponding to the plasma filling a perfectly conducting vessel.

F. *Matrix Evaluation and Diagonalization*

The global functions used in the KERNER code make the evaluation of the matrix elements difficult. Each matrix element involves integration of oscillatory functions over the entire volume. However, by taking advantage of the special analytic equilibrium and an extended algebraic calculation [12], the θ-integration is done accurately. Integrations over ψ are done with high-order Gaussian quadratures.

In the PEST code the matrix elements involve the computation of simple Fourier transforms over well-behaved functions which can be done quickly using a standard Fast-Fourier-Transform routine. Integrations over ψ are done by a composite Simpson's quadrature rule. The ERATO code uses a single-interval rectangular rule in both directions.

In principle, global functions can be found that approximate a given eigenfunction more accurately than local functions, and so yield faster convergence. However, local

functions produce sparse, banded matrices. Thus, local function programs can utilize much larger matrices without loss of efficiency.

A standard eigenvalue package adequately determines all the eigenvalues of the matrix $K^{-1/2}\,\delta W\,K^{-1/2}$ for the smaller matrices associated with the global and mixed Fourier-finite-element methods. For the larger matrices, determination of the structure and growth rate of the most unstable modes is accomplished in all three programs by using an inverse iteration routine [13] that preserves the sparseness of the matrix.

G. *Convergence Studies*

An accurate representation of the eigenvalues and associated eigenfunctions generally demands that a very large number of expansion functions be used. Since this number is limited by the computer memory or other considerations, it is often necessary to extrapolate the results obtained from the use of successive sets of functions. Fortunately, we need only a few points because the extrapolation formulas are simple.

In the KERNER and PEST codes, convergence is studied by varying the number of radial functions M and Fourier components L independently of each other. Usually Ω^2 scales as $\Omega_0^2 - C_L \exp(-\alpha_L L)$ with $\alpha_L \sim 1$ for fixed M, and as $\Omega_0^2 - C_M \exp(-\alpha_M M)$ for KERNER and $\Omega_0^2 - C_M M^{-2}$ for PEST at fixed L. The constants, C_L, α_L, C_M, α_M, can be determined empirically. The exponential convergence is a reflection of the efficacy of a set of analytic functions for representing well-behaved analytic functions.

With the ERATO code, Ω^2 scales at worst as $\Omega^2 = \Omega_0^2 + C_L L^{-2}$ for fixed M and $\Omega^2 = \Omega_0^2 + C_M M^{-2}$ for fixed L. Advantage is usually taken of the fact that convergence of $O(M^{-4})$ can be achieved if $L = M$ for fixed-boundary cases. For free surface modes, the convergence can depend sensitively on the safety factor.

H. *Memory Requirements and Computing Time*

The fundamental limitation on accuracy in these calculations is determined by the number of expansion functions that can be accomodated in the available memory and the processor time on the computer. Of these, for practical purposes, memory requirements for storage of the matrices are usually most severe. For the different methods, the number of nonzero matrix elements which must be calculated and stored scale as

$$S_K \sim 9L^2M^2 + \tfrac{3}{2}LM, \tag{13}$$

$$S_P \sim \tfrac{27}{2}L^2M + \tfrac{3}{2}LM - 9L^2, \tag{14}$$

$$S_F \sim 93LM + 2(L + M). \tag{15}$$

In the implementation, however, some of the sparseness features can not be fully utilized. In practice, the banded matrices do not have to be core resident. Thus, we find that the individual implementations do not differ significantly in total memory requirements, primarily because of other coding factors.

The KERNER code is used on an IBM 360/91 and a DEC PDP-10 machine. Its needed memory space is given by

$$W \approx 50000 + 36(LM)^2 \tag{16}$$

words, where L is the number of Fourier modes in θ and M the number of global test functions in ψ. Typical numbers are $L = 3$, $M = 7$, yielding $W \approx 90000$.

The PEST code is implemented on a CDC-7600, in an overlaid format. In its present version, the memory space scales as

$$W \approx 16000 + L(48L + 64M + 800). \tag{17}$$

Typical numbers are $L = 21$, $M = 32$, yielding $W \approx 96000$ words.

The ERATO code is implemented on a CDC-6500. This code makes extensive use of peripheral memory units. The resident memory space is set by the eigenvalue solver as

$$W \approx 16000 + (L + 1)(32L + 18M + 42). \tag{18}$$

Typical numbers are $L = M = 28$, yielding 58,000 words.

The computing time is set largely by the mapping and the eigenvalue-solver, the latter being common to all three codes. The KERNER code does the mapping analytically and requires little time for this phase. The PEST code has a large grid in ψ, θ and requires

$$T \approx tM, \tag{19}$$

where $t \approx 0.8$ sec on a CDC-7600. A typical value of M would be 48, yielding $T = 40$ sec. This figure could be further optimized, but this is perhaps not of highest priority since the results from one mapping are used many times in the stability studies. The mapping grid for the ERATO code requires fewer flux surfaces, and the time required is reduced by approximately a factor of 2.

The eigenvalue solver is common to all three codes. The cpu time is

$$T \approx 64L^2M(t_1L + t_2N), \tag{20}$$

where N is the number of iterations; $t_1 \approx 52\,\mu$sec and $t_2 \approx 42\,\mu$sec on the CDC-6500. Use of machine coding reduces to t_1 to $26\,\mu$sec. Typical values, $L = M = 28$, yield $T \approx 23$ min. It translates to about 2 min on the CDC-7600.

4. Comparison

Here we discuss several choices of the parameters. These have been chosen primarily to provide tests of the accuracy of the programs, rather than for application to a specific device.

A. *Nearly Straight Circular Column, Fixed-Boundary*

$$\epsilon = 1/20, \quad E = 1, \quad \Lambda = 1, \quad q(0) = 0.08519, \quad n = 10.$$

The spectrum for a fixed-surface case, determined by the PEST code using three Fourier components in θ, $0 \leqslant l \leqslant 2$, and seven finite elements in ψ, and by the KERNER code using seven sets of Bessel functions is shown in Fig. 2. The agreement

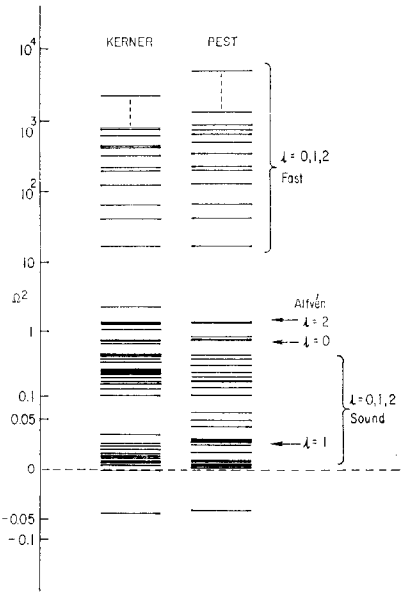

FIG. 2. The spectra obtained from the KERNER and PEST codes for an almost straight, circular plasma with $\epsilon = 1/20$, $E = 1$, $\Lambda = 1$, $q(0) = 0.08519$, $n = 10$. In both cases three Fourier components and seven radial expansion functions are used. The KERNER functions are well suited for the global modes of this case and two unstable modes are found. The second unstable mode appears in PEST when the number of finite elements is increased.

between the calculations is significantly better than that reported earlier [5], thanks to finding a coding error during a detailed study of the discrepancy. There is no significant difference in the values for the discrete modes. The ranges for the continua also agree; the differences in the positions of the sets of modes that represent them are due to the tendency of the global model to localize modes between the zeros of the Bessel functions whereas the finite-element approach places them near equally spaced mesh points in ψ. Exact agreement is obtained by using larger matrices.

B. *Large Aspect Ratio, Nearly Circular Case, Free-Boundary*

$$\epsilon = 1/6, \quad E = 1, \quad \Lambda = 2, \quad n = 1.$$

We consider a free-boundary case with a perfectly conducting wall placed on the surface $\Lambda \equiv (\Psi_W/\Psi_B)^{1/2} = 2$. The growth rate of the most unstable mode is shown in Fig. 3 as a function of q. Converged results are given in Table I for $q(0) = 1.79$ $[q(s) = 2.0]$ and $q(0) = 2.24$ $[q(s) = 2.5]$.

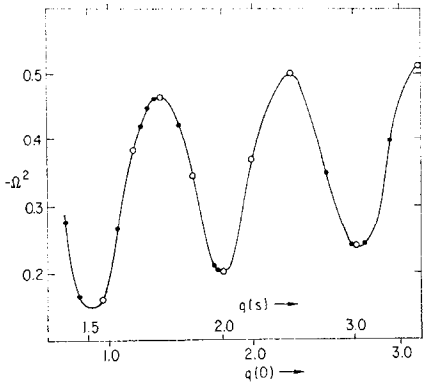

FIG. 3. Plot of $-\Omega^2$ versus q for the case with $\epsilon = \frac{1}{6}$, $E = 1$, $\Lambda = 2$, and $n = 1$. The dots and circles are the results of the KERNER and PEST codes, respectively.

TABLE I

Comparison of Specific Results for the Different Cases[a]

ϵ	E	Λ	$q(0)$	$q(s)$	n	KERNER	PEST	ERATO
$\frac{1}{6}$	1	2	1.7910	2.0	1	0.202	0.204	
$\frac{1}{6}$	1	2	2.2387	2.5	1	0.504	0.506	
$\frac{1}{3}$	2	1	0.3	0.5224	2	0.413	0.427	0.431
$\frac{1}{3}$	2	1	0.7	1.2190	2	0.118	0.119	0.120
$\frac{1}{3}$	2	∞	1.2	2.0897	1		0.75	0.78
$\frac{1}{3}$	2	∞	2.0	3.4829	1		0.68	0.75
$\frac{1}{3}$	2	∞	0.6	1.0449	2		1.31	1.40
$\frac{1}{3}$	2	∞	1.0	1.7415	2		1.03	1.07

[a] Each of these is obtained from convergence studies illustrated by Fig. 5. The eigenvalue Ω^2 is given in terms of the poloidal Alfvén time; $\Omega^2 \equiv \omega^2[\rho q^2(s)R^2/B_0^2]$.

C. *Small Aspect Ratio, Elliptical Case, Fixed-Boundary*

$$\epsilon = 1/3, \quad E = 2, \quad \Lambda = 1, \quad n = 2$$

The growth rate is given as a function of $q(0)$ in Fig. 4. Converged results for the three codes are given in Table I for $q(0) = 0.3$ and $q(0) = 0.7$. Convergence curves are shown in Fig. 5.

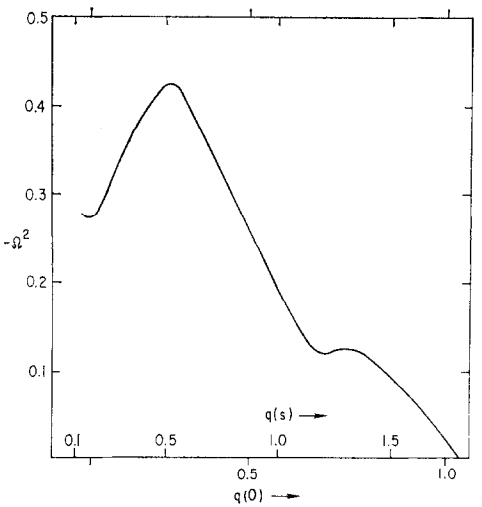

FIG. 4. Plot of $-\Omega^2$ versus q for $\epsilon = \frac{1}{3}$, $E = 2$, $\Lambda = 1$, $n = 2$. The curve is obtained by the ERATO code. The results from all three codes for points at $q(0) = 0.3$ and $q(0) = 0.7$ are compared in Table I.

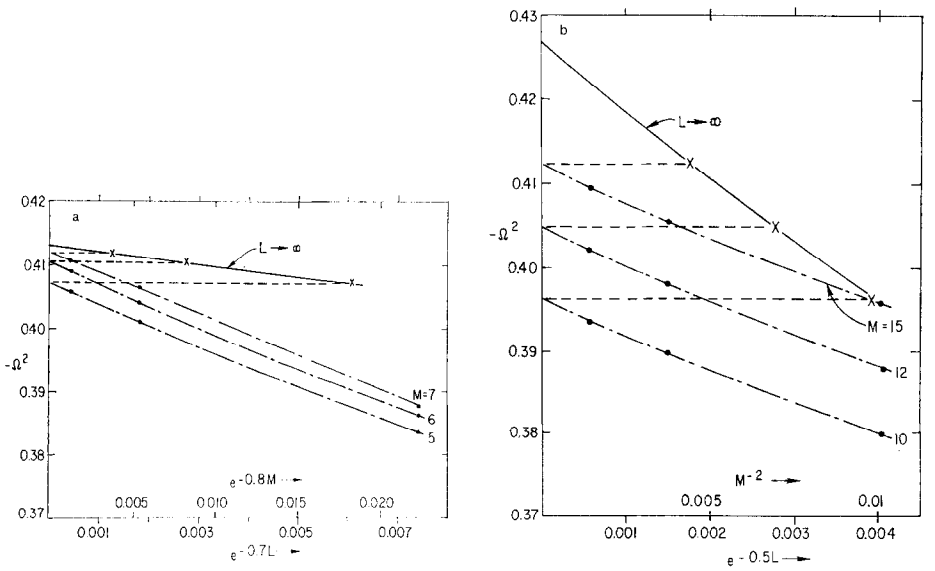

FIG. 5. Illustration of how the results of Table I are obtained for KERNER (a) and PEST (b), where $\epsilon = \frac{1}{3}$, $E = 2$, $\Lambda = 1$, $q(0) = 0.3$, and $n = 1$. The eigenvalues are extraplotated numerically in L for each of three values of M; the resultant values are subsequently extrapolated in M.

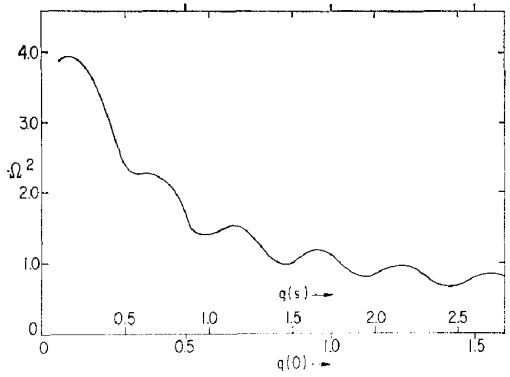

FIG. 6. Plot of $-\Omega^2$ versus q for $\epsilon = \frac{1}{3}$, $E = 2$, $\Lambda = \infty$, $n = 2$. The curve is obtained by the ERATO code. The results from PEST and ERATO are compared in Table I.

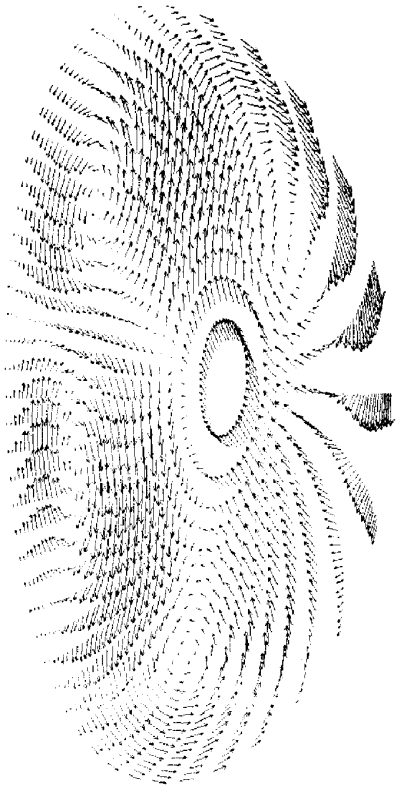

FIG. 7. Projection of the displacement vector onto a constant ϕ plane for the $\epsilon = \frac{1}{3}$, $E = 2$, $\Lambda = 1$, $q(0) = 0.7$, $n = 2$ case, as obtained with the PEST code.

D. *Small Aspect Ratio, Elliptical Case, Free-Boundary*

$$\epsilon = 1/3, \quad E = 2, \quad \Lambda = \infty, \quad n = 1$$

The growth rate for this case is presented in Table 1 for $q(0) = 1.2$ and $q(0) = 2.0$.

E. *Small Aspect Ratio, Elliptical Case, Free-Boundary*

$$\epsilon = 1/3, \quad E = 2, \quad \Lambda = \infty, \quad n = 2.$$

The growth rate for this case is given in Fig. 6, with converged results for $q(0) = 0.6$ and $q(0) = 1.0$ in Table I.

F. *Eigenfunctions*

Reconstruction of the eigenfunctions is useful for the interpretation of results and helps in understanding the physical nature of the modes. The KERNER code lists the coefficients of the different l, ν expansion functions from which such a reconstruction is possible. The PEST code has this feature built into it, and displays the eigenvector or plots of its components as functions of ψ or θ as part of the program. The ERATO code can list the coefficients for constructing a vector plot. Figure 7 shows typical results for the $\epsilon = 1/3, E = 2, \Lambda = 1, q(0) = 0.7, n = 2$ case.

5. Discussion

The purpose of this work is to compare the three codes for a few specified identical equilibria. The good agreement between the results, including both internal and external modes, provides confidence in the accuracy of each of the codes. Indeed, it would be useful to treat these specific cases as standards for comparing the efficacy of other stability codes.

Within the totality of all conceivable ideal MHD stability problems, there are probably many that would test any of these codes. Since the numerical expansion procedures can all be shown analytically to converge asymptotically for the most unstable mode, the most likely source of difference would be in the relative ease in achieving an accurate result, i.e., the number of expansion functions required. Our general experience has shown no regions of parameter space where large differences between the stability results from the three codes should be expected. With respect to an accurate representation of the whole spectrum, it is clear that problems may arise in special cases.

The KERNER code, with its analytic equilibrium and its relatively small matrices, is particularly useful for studies of general physics questions associated with internal modes. However, in small aspect ratio tokamaks, its application to kink instabilities is somewhat limited since the vacuum wall must lie on a constant Ψ-surface of Eq. (3), which is generally close to the plasma–vacuum interface. A large part of its application

has been to the numerical study of the limits of applicability of localized instability criteria [10, 14, 15].

The PEST and ERATO codes are more general in that they can treat numerically determined equilibria, provided that there are no internal separatrices. An outer conducting shell can be placed arbitrarily. This ability to study any aspect of the stability problem brings with it the concomitant difficulty that care must be taken in the interpretation of the results. Very large matrices must often be used and convergence studies are essential.

With the size and cost of experimental devices increasing rapidly, more careful theoretical studies of what should be expected are becoming more and more essential. Thus, these codes have been developed just in time to make an impact on the magnetic fusion energy program.

ACKNOWLEDGMENTS

This work was supported by the U. S. Energy Research and Development Administration Contract EY-76-C-02-3073 with Princeton University and by the Swiss National Science Foundation.

Two of the authors (W.K. and R.G.) appreciate the hospitality extended to them by the Princeton Plasma Physics Laboratory during their stay as Research Associates.

REFERENCES

1. W. KERNER, *Nucl. Fusion* **16** (1976), 643.
2. R. C. GRIMM, J. M. GREENE, AND J. L. JOHNSON, *in* "Methods in Computational Physics," Vol. 16, p. 253, Academic Press, New York, 1976.
3. D. BERGER, L. C. BERNARD, R. GRUBER, AND F. TROYON, paper C3, 2nd European Conference on Computational Physics, Garching (1976).
4. L. S. SOLOV'EV, *Zh. Eksp. Teor. Fiz.* **53** (1967), 626; *Sov. Phys. JETP* **26** (1968), 400.
5. R. C. GRIMM AND J. L. JOHNSON, *Comp. Phys. Commun.* **12** (1976), 45.
6. J. L. JOHNSON, H. E. DALHED, J. M. GREENE, R. C. GRIMM, Y. Y. HSEIH, S. C. JARDIN, J. MANICKAM, M. OKABAYASHI, R. STORER, A. M. M. TODD, D. VOSS, AND K. E. WEIMER, to appear.
7. J. D. CALLEN AND R. A. DORY, *Phys. Fluids* **15** (1972), 1523.
8. I. B. BERNSTEIN, E. A. FRIEMAN, M. D. KRUSKAL, AND R. M. KULSRUD, *Proc. R. Soc. London A* **244** (1958), 17.
9. R. J. TAYLOR, *Proc. Phys. Soc. London B* **70** (1957), 1043.
10. C. MERCIER, *Nucl. Fusion* **1** (1960), 47.
11. R. LÜST AND E. MARTENSEN, *Z. Naturforsch. A* **15** (1960), 706.
12. W. KERNER AND J. STEUERWALD, *Comp. Phys. Commun.* **9** (1975), 337.
13. R. GRUBER, *Comp. Phys. Commun.* **10** (1975), 30; Max-Planck-Institut für Plasmaphysik Report IPP-6/147 (April 1976).
14. J. M. GREENE AND J. L. JOHNSON, *Phys. Fluids* **5** (1962), 510.
15. D. LORTZ AND J. NÜHRENBERG, *Nucl. Fusion* **13** (1973), 821.